Energy Transfer Kinetics of the np(5)(n+1)p Excited States of Ne and Kr

ARTICLE *in* THE JOURNAL OF PHYSICAL CHEMISTRY A · JUNE 2011

Impact Factor: 2.69 · DOI: 10.1021/jp201502m · Source: PubMed

2 AUTHORS, INCLUDING:

Michael Heaven
Emory University
327 PUBLICATIONS **4,358** CITATIONS

SEE PROFILE

THE JOURNAL OF PHYSICAL CHEMISTRY A

ARTICLE

pubs.acs.org/JPCA

Energy Transfer Kinetics of the $np^5(n+1)p$ Excited States of Ne and Kr

Md. Humayun Kabir and Michael C. Heaven*

Department of Chemistry, Emory University, Atlanta, Georgia 30322, United States

ABSTRACT: Energy transfer rate constants for Ne($2p^5 3p$) and Kr($4p^5 5p$) atoms colliding with ground state rare gas atoms (Rg) have been measured. In part, this study is motivated by the possibility of using excited rare gas atoms as the active species in optically pumped laser systems. Rg($np^5(n+1)s$) metastable states may be produced using low-power electrical discharges. The potential then exits for optical pumping and laser action on the $np^5(n+1)p \leftrightarrow np^5(n+1)s$ transitions. Knowledge of the rate constants for collisional energy transfer and deactivation of the $np^5(n+1)p$ states is required to evaluate the laser potential for various Rg + buffer gas combinations. In the present study we have characterized energy transfer processes for Ne ($2p^5 3p$) + He for the six lowest energy states of the multiplet. Rate constants for state-to-state transfer have been determined. Deactivation of the lowest energy level of Kr ($4p^5 5p$) by He, Ne, and Kr has also been characterized. Initial results suggest that Kr ($4p^5 5p$) + Ne mixtures may be the best suited for optically pumped laser applications.

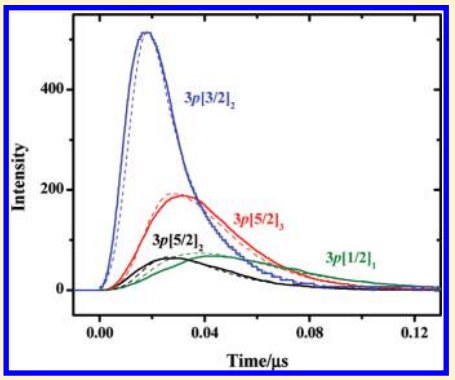

INTRODUCTION

In recent years there have been concerted efforts to develop high energy optically pumped alkali vapor lasers.[1−5] These devices utilize excitation of the $^2P_{3/2} \leftarrow {}^2S_{1/2}$ transition, followed by collisional relaxation and lasing on the $^2P_{1/2} \rightarrow {}^2S_{1/2}$ line. There is interest in using elements other than the alkali metals for this type of laser to expand the range of pump and lasing wavelength that can be employed. However, the alkali metals are somewhat unique in terms of their suitability for optically pumped laser applications. The properties that make them so favorable, which include the low temperatures needed to obtain sufficient vapor pressures and the presence of low energy allowed transitions are not offered by any other group in the periodic table. Ionization of the group II metals yields ions with the same electronic configuration as the alkali metals, but there are obvious problems with this approach. The vaporization temperatures for the alkaline earths are higher compared to the alkali's, it is difficult to generate high number densities of ions, and the $^2P-{}^2S$ transitions are at higher energies. An alternative strategy is to use optical pumping of atoms that are in metastable electronic states. Production of the metastable atoms can be accomplished using optical or electric discharge excitation. The basic concept of an optically pumped laser that utilizes metastable atoms in this way was demonstrated for Hg* by Holmes and Siegman,[6] and Burnham and Djeu.[7] These investigators used optical excitation to excite the $6s6p\ ^3P_1$ and $^3P_0$ metastable levels. Lasing was achieved through optical pumping of the $6s7s\ ^3S_1-6s6p\ ^3P_0$ transition.

The $np^5(n+1)s$ configurations of rare gas atoms support metastable $ns[3/2]_2$ and $ns'[1/2]_0$ states (Racah notation) that are readily populated under mild electric discharge conditions. Strongly allowed optical transitions connect these levels to states of the $np^5(n+1)p$ manifold. In principle, these $(n+1)p \leftarrow (n+1)s$ transitions can be used for optically pumped laser applications, if the states involved exhibit suitable collisional relaxation kinetics. To be more specific, the $np^5(n+1)p$ configuration gives rise to ten electronic states. In the following we label these states using the Racah notation, $nl[K]_J$, where $K = J_{core} + l$ and $J = K + S$. The J_{core} quantum number is associated with the electronic angular momentum of the $Rg^+ np^5$ core configuration which gives rise to a widely split, inverted ^2P state. The lower energy component has $J_{core} = 3/2$, which, when combined with the $(n+1)p$ outer electron, gives rise to six states (designated by $(n+1)p$). Combining $J_{core} = 1/2$ with the $(n+1)p$ outer electron produces a further four states that are designated by $(n+1)p'$. A laser scheme that mimics the alkali vapor system would be to excite the $3p[5/2]_3 \leftarrow 3s[3/2]_2$ transition and lase on the $3p[1/2]_1 \rightarrow 3s[3/2]_2$ line. This scheme has a level degeneracy advantage as the $3p[5/2]_3$ and $3p[1/2]_1$ levels have degeneracies of 7 and 3, respectively.

In the present study, we have examined the energy transfer kinetics of Ne($2p^5 3p$) and Kr($4p^5 5p$) to assess the potential for using these species as the upper levels of optically pumped lasers. The results for Ne($2p^5 3p$) are the most developed, and constitute the primary topic of this paper. Preliminary results for Kr($4p^5 5p$) are also presented.

Due to the high internal energy of metastable Ne, most collision partners will undergo Penning ionization which provides a very efficient quenching channel. Therefore we consider collisions of Ne($2p^5 3p$) with He and Ne, where Penning ionization cannot occur. Ne($2p^5 3p$) + Ne collisions have been studied by

Special Issue: David W. Pratt Festschrift

Received: February 15, 2011
Revised: May 20, 2011
Published: June 13, 2011

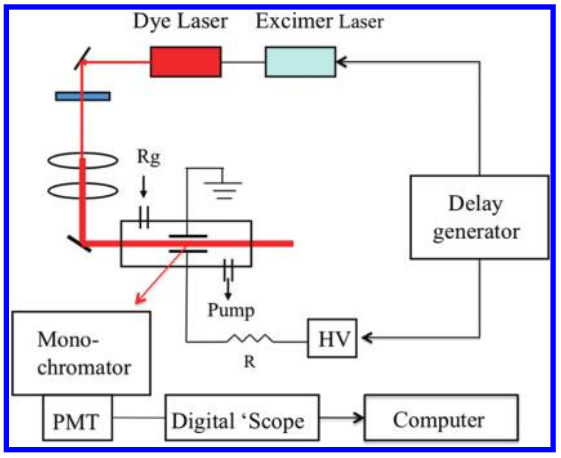

Figure 1. Schematic diagram of the apparatus used to observe Rg* fluorescence decay kinetics.

several investigators.[8−11] Chang and Setser[12] found that the $3p[1/2]_1$ level is quenched (loss to levels outside of the $2p^5 3p$ manifold) with a rate constant of 1.7×10^{-11} cm^3 s^{-1}, which is too fast for the proposed application. Collisions between Ne($2p^5 3p$) and He have also been examined,[8,9,13−18] but all of the state-to-state transfer measurements have focused on the higher energy levels (in part because the 632.8 nm line of the HeNe laser terminates on the $3p'[3/2]_2$ level). Based on an analysis of the emissions from high pressure He−Ne mixtures, Batyrbekov et al.[19] estimated that the rate constant for the quenching of Ne($2p^5 3p$) by He was less than 10^{-13} cm^3 s^{-1}. In the following we present the first experimental study of Ne($2p^5 3p$) + He state-to-state energy transfer for the lower energy levels (mostly $J_{core} = 3/2$).

Kr($4p^5 5p$) metastables carry less energy than Ne($2p^5 3p$), so the range of collision partners that will not be ionized is greater. We have obtained preliminary data for collisional deactivation of Kr($4p^5 5p$) $5p[1/2]_1$ by He, Ne, and Kr. Transfer induced by collisions of Kr($4p^5 5p$) with Ar was studied previously by Chang et al.[20]

EXPERIMENTAL SECTION

Figure 1 shows a schematic diagram of the experimental apparatus used to investigate the kinetics of Rg($np^5(n+1)p$) + Rg′ collisions. A pulsed discharge is used to generate Rg($np^5(n+1)s$) metastables, which are then excited to specific Rg($np^5(n+1)p$) levels using a pulsed laser. A cylindrical (L = 10 cm and W = 4 cm) Pyrex discharge cell was used to contain the slowly flowing rare gas mixtures. Fused silica windows were attached to the ends of the cylindrical cell. A pair of stainless steel parallel-plate electrodes was mounted by tungsten rods inside the cell with a 2.0 cm interelectrode spacing. A negative pulsed dc voltage of 500−800 V was applied across the electrodes to generate the discharge plasma. The discharge period was 350 μs, the repetition rate was 10 Hz, and the maximum peak current ranged from 150 to 350 mA.

A rotary pump was used to evacuate the cell to a base pressure of 1.0 mTorr. Ultrahigh purity grade (99.999%) neon, krypton, and helium was used. These gases were further purified by passage through molecular sieve traps that were immersed in liquid nitrogen. The total gas pressure in the discharge cell was measured by a capacitance manometer (MKS Baratron).

Tunable radiation with spectral bandwidth of 0.3 cm^{-1} was produced from a dye laser pumped by the 308 nm output of an excimer laser running at 10 Hz (Lambda Physik EMG201/FL3002). The line width was determined from laser excitation spectra for the metastable Ne. A range of dye solutions (Rhodamine 610, Rhodamine 640, Oxazine 720, LDS 798, and LDS 867 laser dyes) were used to cover a wavelength range from 600 to 894 nm to excite the $3p[3/2]_2$, $3p[3/2]_1$, $3p[5/2]_2$, $3p[5/2]_3$, and $3p[1/2]_1$ levels of Ne($2p^5 3p$), and the $5p[1/2]_1$ level of Kr($4p^5 5p$).

The output from the dye laser was directed between the electrodes in the discharge cell. Fluorescence was collected along an axis that was perpendicular to the laser light propagation. A biconvex lens was used to focus the fluorescence onto the entrance slit of a 0.64 m monochromator (Instruments SA HR-640, 1200 g/mm grating). At the exit slit, the dispersed fluorescence was detected by a photomultiplier tube (PMT) (RTL, B2/RFI). The output from the PMT was processed by a boxcar integrator (Stanford Research Systems, SR 250) for the recording of emission spectra. Time resolved signals were recorded with the monochromator set to transmit the light from a single emission line. The temporal profiles were captured by a 150 MHz oscilloscope (Tektronix TDS 1012). Typically, 128 laser shots were averaged to obtain results with good signal-to-noise ratios. For the analysis of the peak intensity data of the emission spectra, knowledge of the wavelength dependence of the relative detection efficiency was need. Variation of the response of the monochromator/PMT combination in the 600−900 nm region was calibrated using a tungsten lamp.

All measurements for Ne were made with the laser set to excite the metastables 450 μs after the cessation of the discharge. The delay of the dye-laser pulse relative to the termination of the electrical discharge was controlled by a digital delay generator (Stanford Research Systems DG535). Time-resolved fluorescence signals for Ne ($2p^5 3p$) at varying pressures of the He buffer gas were recorded to obtain total depopulation rate constants for a chosen initial level. Time integrated fluorescence spectra were measured by fixing the dye laser wavelength on a specific $2p^5 3p$−$2p^5 3s$ transition and scanning the monochromator through the region that covered the emission lines of the initially populated state and those of the levels populated by collisional energy transfer. A boxcar gate width of 100 ns was used for these measurements. These spectra were corrected for the wavelength dependent response of the detection system.

Measurements of Kr($4p^5 5p$) + Rg transfer rate constants for Rg = He, Ne, and Kr were carried out using the techniques described above. The deactivation of Kr ($4p^5 5p$) $5p[1/2]_1$ was examined using excitation of the $5p[1/2]_1 \leftarrow 5s[3/2]_2$ transition (892.9 nm) followed by detection of the $5p[1/2]_1 \rightarrow 5s[3/2]_1$ line (975.2 nm). Relatively rapid decay of the Kr ($4p^5 5s$) metastables was observed at the termination of the discharge pulse. Owing to this circumstance, the laser induced fluorescence (LIF) measurements were made during the discharge pulse.

RESULTS AND ANALYSIS

Emission Spectra of the Neon Discharge. As an initial step used to partially characterize the discharge and calibrate the wavelength drive of the monochromator, the emission spectrum produced by discharge excitation of Ne was recorded for the range 580−680 nm. Figure 2 shows a spectrum for 2.5 Torr of pure Ne excited by a pulsed discharge at 800 V. All of the prominent emission lines in this trace correspond to $2p^5 3p$−$2p^5 3s$

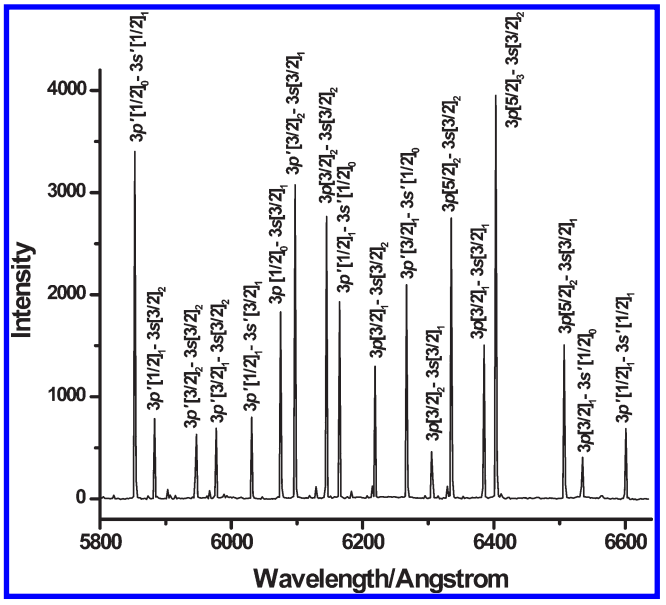

Figure 2. Emission spectrum produced by an 800 V discharge in 2.5 Torr of pure Ne.

transitions, and the assignments are indicated. Figure 2 shows that the resolution of the monochromator was sufficient to permit selective detection of the emission from individual levels of the $2p^5 3p$ multiplet.

Total Helium Deactivation Rate Constants for the Ne $2p^5 3p$, $J_{core} = 3/2$ States. We have measured the total depopulation for the five lowest energy Ne($2p^5 3p$), $J_{core} = 3/2$ states. All of these states are optically connected to the states of the Ne ($2p^5 3s$) configuration by electric dipole allowed transitions. Laser excitation occurred 450 μs after the discharge, by which time the fluorescence from the discharge excited plasma had decayed to an insignificant level. However, the Ne ($2p^5 3s$) levels are long-lived, and a substantial concentration of metastable Ne was present at the chosen delay. From optical absorption measurements, made with the dye laser tuned to the center of the $3p[3/2]_2 - 3s[3/2]_2$ line, the density of the metastable states in our experiment was estimated to be on the order of 10^{11} cm^{-3}.

The total depopulation rate constant for transfer out of a selected Ne($2p^5 3p$) level was measured by time-resolving the fluorescence from the initially excited level. Where possible, the emission line monitored was not the same as the excitation line in order to avoid interference from scattered laser light. As an example, Figure 3 shows the fluorescence signal obtained by excitation of the $3p[3/2]_2 \leftarrow 3s[3/2]_2$ transition with detection of the $3p[3/2]_2 \rightarrow 3s'[1/2]_1$ emission. Note that the curve shows a finite rise time and rounded maximum (Figure 3a) because the duration of the excitation pulse is comparable to the fluorescence decay lifetime. As described below, the temporal profile of the laser pulse can be modeled as a Gaussian function with a full width at half-maximum (fwhm) of 12 ns. Consequently, the segment of the decay curve starting 10 ns after the maximum of the laser pulse was used to characterize the fluorescence decay rate. Figure 3b show a semilog plot of this segment of the data, along with the line generated by fitting a single exponential decay function to the data (the stepped behavior of the data at long decay times is an artifact due to the limited accuracy of the analog to digital conversion). This example gave a good fit to a single exponential decay, as did the corresponding curves for

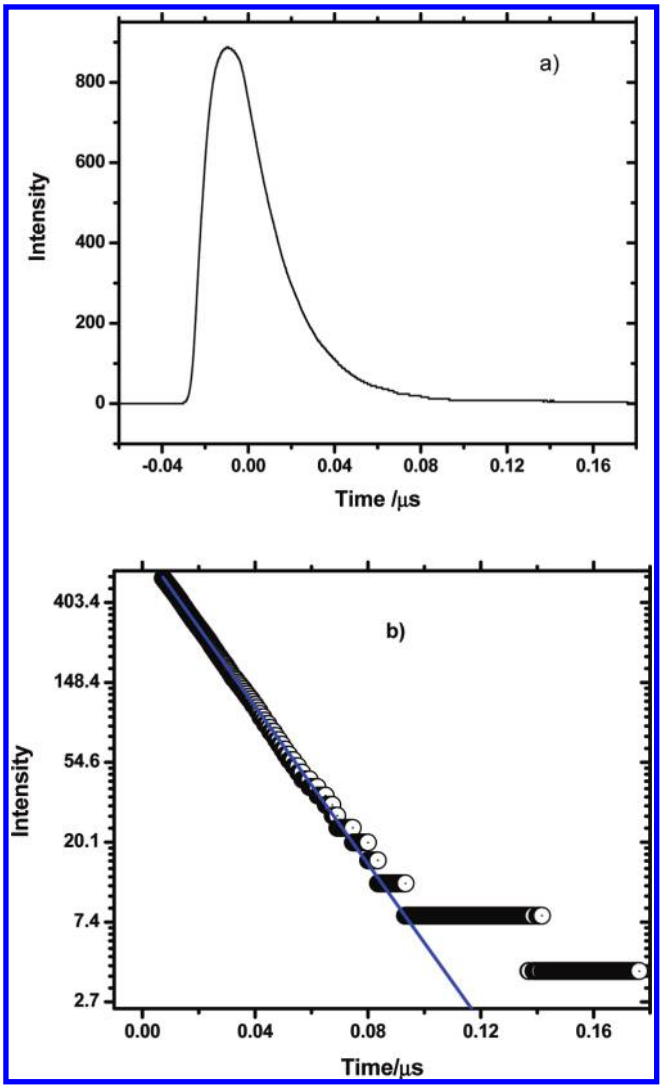

Figure 3. Fluorescence decay curves for the $3p[3/2]_2$ level of Ne-($2p^5 3p$)in the presence of Ne (1.4 Torr) and He (8.5 Torr). The line in trace b is a fitted single exponential decay function. The stepped behavior of the data at long decay times is an artifact due to the limited accuracy of the analog to digital conversion.

population transfer out of the other Ne($2p^5 3p$) levels examined in this study.

The observation of single exponential decay kinetics indicates that back transfer into the initially populated level is unimportant. Hence, the decay of population from an initially populated state i can be represented by the expression

$$[i] = [i]_0 \exp(-R_{T,i}t) \quad (1)$$

where $[i]$ indicates the concentration of state i, $[i]_0$ is the initial concentration at time $t = 0$ (defined by the effective end of the laser pulse), and $R_{T,i}$ is the total removal rate. The latter is defined by

$$R_{T,i} = \Gamma_{rad} + (k_{q,i}^{He} + \sum_f k_{f,i}^{He})[He] + (k_{q,i}^{Ne} + \sum_f k_{f,i}^{Ne})[Ne] \quad (2)$$

where Γ_{rad} is the radiative decay rate and $k_{f,i}^{M}$ is the rate constant for transfer from state i to final state f induced by collision with the species M (He or Ne). The rate constants for transfer to levels that are not members of the $2p^5 3p$ multiplet are designated by $k_{q,i}^{M}$. In

dx.doi.org/10.1021/jp201502m |J. Phys. Chem. A 2011, 115, 9724–9730

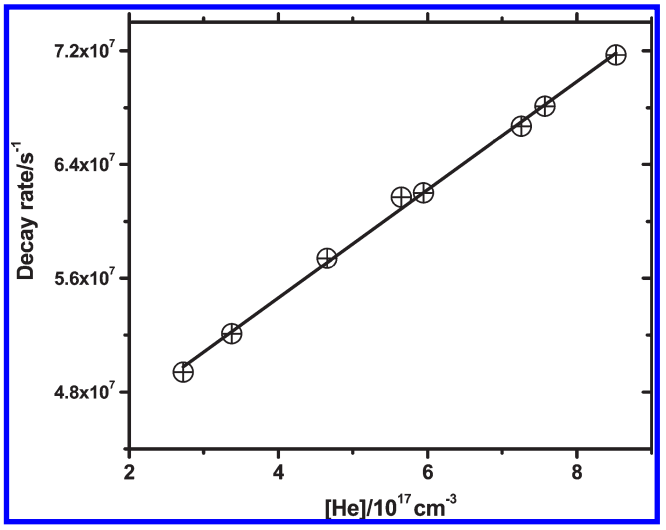

Figure 4. Dependence of the Ne($2p^5 3p$)$3p[3/2]_2$ fluorescence decay rate on [He] with [Ne] held constant at 4.5×10^{16} cm^{-3}.

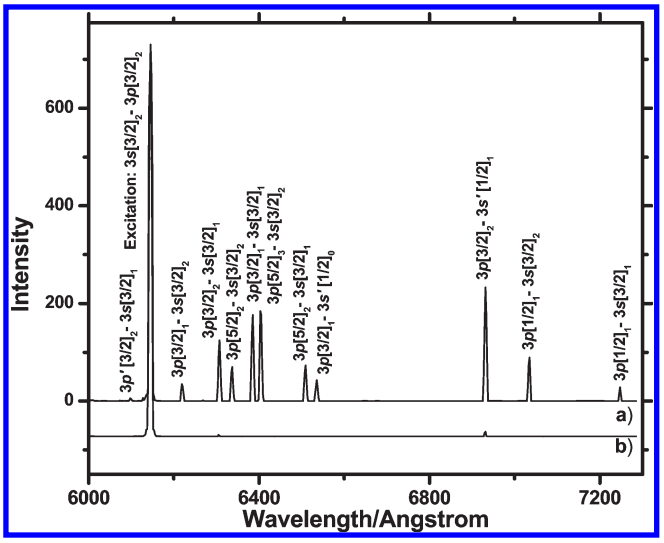

Figure 5. Time-integrated fluorescence spectra resulting from laser excitation of the Ne($2p^5 3p$) $3p[3/2]_2$ level. Trace (a) is for 1.4 Torr of Ne with 26.6 Torr of He. Trace (b) shows the spectrum for 1.4 Torr of pure Ne.

Table 1. Total Removal Rate Constants for Ne($2p^5 3p$) with He and Ne

	Ne($2p^5 3p$) + He, present work	Ne($2p^5 3p$) + Ne, ref 12
level	k_T^{He} (10^{-11} cm^3 s^{-1})	k_T^{Ne} (10^{-11} cm^3 s^{-1})
$3p[3/2]_2$	3.8 ± 0.5	1.2 ± 0.4
$3p[3/2]_1$	4.7 ± 1.0	0.9 ± 0.2
$3p[5/2]_2$	4.5 ± 1.0	1.8 ± 1.4
$3p[5/2]_3$	6.3 ± 1.2	4.4 ± 1.1
$3p[1/2]_1$	1.7 ± 0.3	1.7 ± 0.5

the following, we denote the rate constant for total removal of population from state i by collisions with He as

$$k_{T,i}^{He} = k_{q,i}^{He} + \sum_f k_{f,i}^{He} \quad (3)$$

To determine the $k_{T,i}^{He}$ values, total decay rates were measured for He pressures in the range of 10−30 Torr, with the Ne pressure held constant (at 1.4 Torr for most cases). For these data, plots of $R_{T,i}$ versus [He] (often referred to as a Stern−Volmer plot), such as the example shown in Figure 4, have a slope of $k_{T,i}^{He}$ and intercept of $\Gamma_{rad} + k_{T,i}^{Ne}$ [Ne]. The He total removal rate constants determined from this model are listed in Table 1. For comparison, Table 1 also includes the Ne total removal rate constants determined by Chang and Setser.[12]

He + Ne($2p^5 3p$) State-to-State Transfer Rate Constants. A combination of time- and wavelength-resolved fluorescence measurements were used to characterize the collisional transfer processes following single-level excitation of Ne($2p^5 3p$). Figure 5 shows time-integrated resolved fluorescence spectra recorded using initial excitation of the $3p[3/2]_2$ level. For trace (a) the pressures of He and Ne were 26.6 and 1.4 Torr, respectively. The large excess of He ensured that the majority of transfer events were a consequence of Ne($2p^5 3p$) + He collisions. Figure 6 shows the time-resolved fluorescence profiles for the same experiment. Data of this kind were taken for all initial levels in the range $3p[3/2]_2$−$3p[1/2]_1$.

Analysis of the state-to-state transfer data was conducted in two stages. First, an approximate analytical model was applied to

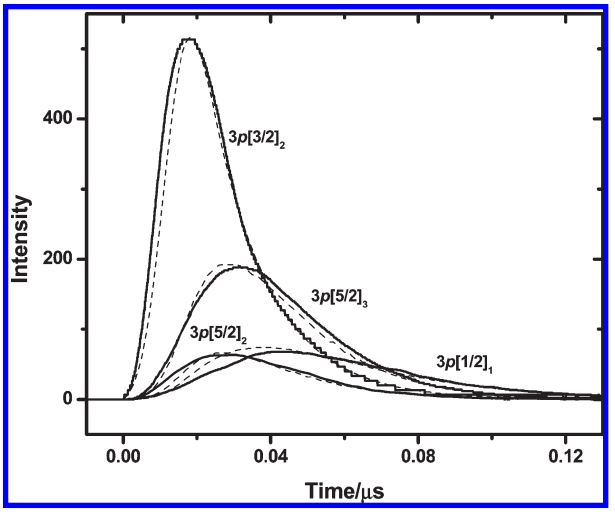

Figure 6. Time-resolved fluorescence signals following excitation of Ne($2p^5 3p$) $3p[3/2]_2$ in the presence of 1.4 Torr of Ne and 26.6 Torr of He.

extract a preliminary set of rate constants. These were then used as the starting values for full master equation simulations of the time- and wavelength-resolved fluorescence data. The final rate constant set was obtained by systematic adjustment of the rate constants in the numerical simulations.

To obtain analytical expressions for the time-dependent state populations, we start by considering a model where all back-transfer processes are neglected. The initially populated level can only loose population, and the collisionally populated levels only receive population from the initially excited state. This is a good approximation when the number of transfer collisions experienced during radiative decay is small. For this assumption the time dependence of $[i]$ is given by eq 1 above. The rate equation for a collisionally populated level is given by

$$\frac{d[f]}{dt} = R_{f,i}[i] - R_{T,f}[f] \quad (4)$$

dx.doi.org/10.1021/jp201502m |J. Phys. Chem. A 2011, 115, 9724–9730

Table 2. Energy Transfer Rate Constants for $Ne(2p^5 3p) + He$[a]

$i \setminus f$	$3p'[3/2]_2$	$3p'[3/2]_1$	$3p[3/2]_2$	$3p[3/2]_1$	$3p[5/2]_2$	$3p[5/2]_3$	$3p[1/2]_1$	$\Sigma k_{i,f}$	$k_{q,i}$
$3p[3/2]_2$	0.0	0.03	0.0	1.3	0.8	0.9	0.7	3.7	0.0
$3p[3/2]_1$	0.01	0.02	0.9	0.00	1.1	1.7	1.4	5.1	0.0
$3p[5/2]_2$	0.0	0.0	0.08	0.2	0.0	2.8	2.3	5.4	0.6
$3p[5/2]_3$	0.0	0.0	0.03	0.08	0.8	0.0	1.9	2.8	3.4
$3p[1/2]_1$	0.0	0.0	0.0	0.0	0.002	0.005	0.00	0.007	1.7

[a] Units are 10^{-11} cm^3 s^{-1}. Errors are estimated to be 25%.

with $R_{f,i} = k_{f,i}^{He}[He] + k_{f,i}^{Ne}[Ne]$. Substitution of eq 1 in eq 4 and integration yields the expression

$$[f] = \frac{R_{f,i}[i]_0}{(R_{T,i} - R_{T,f})}(\exp(-R_{T,f}t) - \exp(-R_{T,i}t)) \quad (5)$$

The time-integrated fluorescence spectra have line intensities that are proportional to the time-integrated level populations. As the boxcar gate width was sufficient to collect >90% of the emitted light, we can approximate the time-integrated populations by

$$P_i = \int_0^\infty [i]dt = \frac{[i]_0}{R_{T,i}} \quad \text{and}$$
$$P_f = \int_0^\infty [f]dt = \frac{R_{f,i}[i]_0}{R_{T,i}R_{T,f}} \quad (6)$$

The ratios of these terms are then related to the ratios of the time-integrated fluorescence intensities by the expression

$$\frac{P_f}{P_i} = \frac{R_{f,i}}{R_{T,f}} = \frac{(I_{f,l}/A_{f,l})}{(I_{i,l'}/A_{i,l'})} \quad (7)$$

where $I_{f,l}$ is the observed intensity of the transition from state f to the lower level l (after correcting for the instrumental response function) and $A_{f,l}$ is the radiative decay rate for the $f \rightarrow l$ transition. The values determined by Chang and Setser[11] were used for the radiative decay rates. The rates in eq 7 include contributions from collisions with both He and Ne. However, as the spectra were recorded under conditions with [He] ≫ [Ne], the contributions from $Ne(2p^5 3p)$ + Ne collisions were neglected at this stage of the analysis. The justification for this neglect is apparent in trace (b) of Figure 5, where the extent of transfer observed for Ne alone is minimal. With this additional approximation the state-to-state rate constants can be estimated from the expression

$$k_{f,i}^{He} \approx \frac{(I_{f,l}/A_{f,l})}{(I_{i,l'}/A_{i,l'})}k_{T,i}^{He} \quad (8)$$

Preliminary state-to-state rate constants were derived using eq 8. Estimates for the $k_{q,i}^{He}$ rate constants were obtained by application of eq 3.

Master equation modeling was used to refine the rate constants. The coupled differential rate equations for this problem are given by

$$\frac{d[i]}{dt} = S(t) + \sum_n R_{i,n}[n] - R_{T,i}[i] \quad (9)$$

and

$$\frac{d[f]}{dt} = \sum_n R_{f,n}[n] - R_{T,f}[f] \quad (10)$$

where $S(t)$ defines the excitation of the initial state by the laser pulse. This was represented by a Gaussian function with a fwhm of 12 ns. The contributions from $Ne(2p^5 3p)$ + Ne collisions were included using the rate constants of Chang and Setser.[12]

Equations 9 and 10 were solved by standard numerical integration techniques. The results were used to simulate both the time- and wavelength-resolved fluorescence data. As exothermic transfer was generally more efficient than endothermic transfer, the strategy for refining the rate constants was to start with data for initial excitation of the lowest energy level ($3p[1/2]_1$) and progress to initial states with successively higher energies. Transfer from $3p[1/2]_1$ to other states in the $2p^5 3p$ manifold was inefficient, such that almost all of the population loss could be attributed to transfer to other multiplet states (i.e., $k_{q,x}^{He} \approx k_{T,x}^{He}$, $x = 3p[1/2]_1$). Going to higher energies, the numbers of levels significantly involved in the energy transfer processes increased. However, the number of rate constants to be modified at each step was kept to a minimum as the subset of rate constants for the lower levels had already been subject to an iteration of refinement. The state-to-state rate constants were constrained using the principle of detailed balance and refined by performing multiple optimization cycles.

As examples of the quality of the final fits obtained from the master equation model, comparisons of the measured and simulated data for $i = 3p[3/2]_2$ for the time-resolved fluorescence data are presented as the broken curves in Figure 6. Note that the intensities in Figure 6 are arbitrary, and it is the fit to the time dependence that was optimized. The optimized rate constants for $Ne(2p^5 3p)$ + He energy transfer are collected in Table 2.

Kr($4p^5 5p$) + Rg Total Removal Rate Constants for the $5p[1/2]_1$ Level. Loss of population from the Kr $5p[1/2]_1$ level was observed using pure Kr pressures in the range of 2.0−5.5 Torr for collisions with ground state Kr. Deactivation by He and Ne was characterized using a Kr pressure of 0.1 Torr, with collision gas pressures in the range of 10−20 Torr. In all cases, the $5p[1/2]_1$ fluorescence decay curves exhibited single exponential decay kinetics after the termination of the laser pulse. Stern−Volmer plots were used to determine the total removal rate constants. Representative data for He, Ne, and Kr are shown in Figure 7. Here it can be seen that deactivation by Kr was much faster than the transfer processes induced by the lighter rare gases. The deactivation rate constants were found to be $k_{T,10}^{He} = 6 \times 10^{-12}$, $k_{T,10}^{Ne} \leq 2 \times 10^{-12}$, and $k_{T,10}^{Kr} = 7 \times 10^{-11}$ cm^3 s^{-1}.

DISCUSSION

The total removal rate constants for $Ne(2p^5 3p)$ + He reported here are similar in magnitude to the $Ne(2p^5 3p)$ + Ne removal rate constants of Chang and Setser[12] (c.f. Table 1). The most notable deviation is for $3p[3/2]_1$, which shows a surprisingly small rate constant for collisions with Ne.

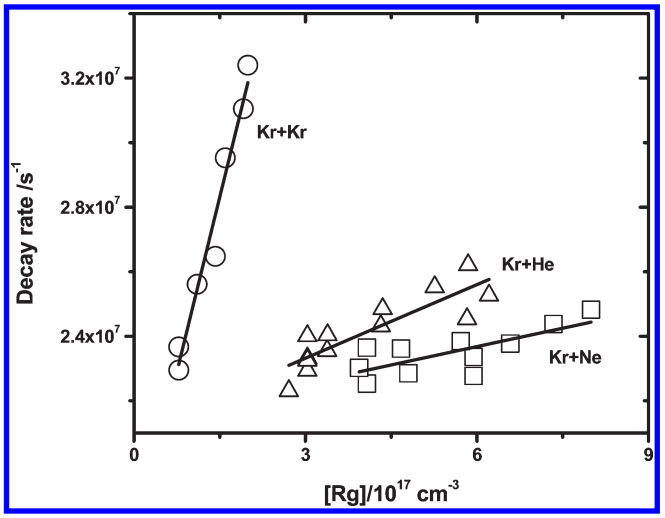

Figure 7. Stern−Volmer plots for the deactivation of Kr($4p^5 5p$) $5p$-$[1/2]_1$ by collisions with He, Ne, and Kr.

Table 3. Comparison of Ne($2p^5 3p$) + He Energy Transfer Cross Sections (Å^2)

$f-i$	$\sigma_{f,i}$, present work	$\sigma_{f,i}$, ref 17
$3p[3/2]_2-3p'[3/2]_1$	0.3	0.8
$3p[3/2]_1-3p[3/2]_2$	1.0	4.7
$3p[3/2]_1-3p'[3/2]_1$	0.01	0.3
$3p[3/2]_2-3p[3/2]_1$	0.6	3.2
$3p[5/2]_2-3p[3/2]_1$	0.8	9.0
$3p[1/2]_1-3p[5/2]_2$	1.8	1.9
$3p[1/2]_1-3p[5/2]_3$	1.4	2.5

Although there have been previous studies of Ne($2p^5 3p$) + He energy transfer, there are no processes for which direct comparisons can be made. Arrathoon and Sealer[13] examined the total removal rate constant for Ne $3p'[3/2]_2$ + He. Their decay rate data (Figure 5 of ref 13) yields a rate constant of 11×10^{-11} cm^3 s^{-1}. Hennecart et al.[8,9,15] and Webster and Shaw[21] examined transfer between the higher energy levels. At a temperature of 300 K, the state-to-state transfer rate constants they obtained for exothermic transfer between adjacent levels were appreciably larger than the range of values we report in Table 2. For example, the rate constant for transfer from $3p'[3/2]_2$ to $3p'[3/2]_1$ was found to be 10.4×10^{-11} cm^3 s^{-1} (ref 21).

Manders et al.[16−18] used crossed molecular beam techniques to examine Ne($2p^5 3p$) + He collisions. They observed transfer from the initial levels $3p'[1/2]_1$, $3p'[3/2]_1$, $3p[3/2]_2$, $3p[3/2]_1$, $3p[5/2]_2$, and $3p[5/2]_3$ to the final levels $3p'[3/2]_2$, $3p'[3/2]_1$, $3p[3/2]_2$, $3p[3/2]_1$, $3p[5/2]_2$, and $3p[1/2]_1$. These experiments were conducted at a fixed collision energy, yielding data that are not directly comparable to the thermally averaged rate constants obtained in the present study. The molecular beam experiments provide collision cross sections ($\sigma_{f,i}$). These may be compared to the thermal rate constants using the approximate expression

$$\sigma_{f,i} = k_{f,i}/\langle v \rangle \qquad (11)$$

where $\langle v \rangle$ is the average velocity for the collision pair (1.369×10^5 cm s^{-1} for Ne + He at 295 K). Ideally, the conversion should be made for a collision energy that corresponds to the average velocity. However, the molecular beam measurements were made at a collision energy of 807 cm^{-1}, while the average thermal energy was 205 cm^{-1}.

Table 3 compares the transfer cross sections of Manders et al.[17] with those derived by converting the rate constants from Table 2 into cross sections. In all cases, the molecular beam cross sections are greater than those derived from our room temperature measurements. This may indicate that the higher energy collisions of the molecular beam experiments can reach potential energy curve crossings that are not accessible for the majority of collisions that are governed by a 295 K thermal distribution. Note that the greatest disagreements are found for transfer from the $3p[3/2]_1$ level. Whereas Chang and Setser[12] found this level to be quite resistant to transfer in Ne($2p^5 3p$) + Ne collisions, the results of Manders et al.[17] suggest that transfer out of $3p[3/2]_1$ is collisions with He is particularly facile.

Hennecart[8] used a temperature controlled cell to examine the Ne($2p^5 3p$) + He transfer processes $3p[1/2]_0 \leftrightarrow 3p'[3/2]_2$ and $3p'[3/2]_2 \leftrightarrow 3p'[3/2]_1$ (labeled as $3 \leftrightarrow 4$ and $4 \leftrightarrow 5$ in ref 8). The cross sections obtained at 300 K were $\sigma_{4,3} = 60$, $\sigma_{3,4} = 9$, $\sigma_{5,4} = 7.3$, and $\sigma_{4,5} = 8.7$ Å^2. These values are much larger than the cross sections derived from our results for lower energy levels, but measurements for common initial levels are needed to see if the data from these two studies are consistent.

Theoretical predictions of the of the Ne($2p^5 3p$) + He energy transfer cross sections have been made using quantum scattering calculations.[9,14,17] The first problem with this type of calculation is that it is difficult to determine the relevant potential energy curves. Approximate curves have been generated by using ab initio electronic structure methods to characterize the $HeNe^+$ core for the collision complex. The potentials for the neutral collision pair were then constructed by treating the interaction of a single valence electron with the molecular ion core. Hennecart and Masnou-Seeuws[9] used this approach to calculate cross sections for the $3p[1/2]_0 \leftrightarrow 3p'[3/2]_2$ and $3p'[3/2]_2 \leftrightarrow 3p'[3/2]_1$ transitions. Collisions that sampled interatomic separations greater than 4.5 a_0 were considered in this model, and reasonable agreement with the experimental results of Hennecart[8] was obtained. The model was improved by Manders et al.,[17] who extended the potential energy curves to collision distances smaller than 4.5 a_0. Full close coupled scattering calculations that employed these potentials produced transfer cross sections that were in reasonable agreement with the crossed beam measurements.

The implications of the present measurements do not appear to be favorable for the optically pumped laser scheme proposed in the introduction (optical pumping of $3p[5/2]_3$ with lasing from $3p[1/2]_1$). Although the rate constant for He-induced transfer from $3p[5/2]_3$ to $3p[1/2]_1$ is suitably large, the rate constants for quenching to states outside of the $2p^5 3p$ manifold are of a comparable magnitude. Consequently, the laser would have a low efficiency and a large fraction of the pump energy would be converted into heat in the lasing medium. However, in this context, it is interesting to note that lasing on the $3p[1/2]_1 \rightarrow 3s[3/2]_2$ transition has been observed when high-pressure (>1 atm) Ne−He mixtures were subjected to pulsed e-beam excitation.[22] The results suggest that the *effective* transfer rate constants for high pressure conditions differ from the values observed in the low-pressure, binary collision limit.

Deactivation of Kr($4p^5 5p$) $5p[1/2]_1$ by Kr was found to be quite efficient, with a rate constant that was close to the value

reported by Chang et al.[20] for collision with Ar ($k_{T,x}^{Ar}$ = 12.2 × 10^{-11} cm^3 s^{-1}). Population transfer induced by collisions with the lighter rare gases was at least an order of magnitude slower. For Ne the process was slow enough that the present measurement should be viewed as an upper bound. Transfer from $5p[5/2]_3$ to $5p[1/2]_1$ in $Kr(4p^5 5p)$ + He collisions was briefly examined, and the rate constant is approximately k^{He} = 1.2 × 10^{-11} cm^3 s^{-1}. The information obtained so far indicates that further studies of the potential of using $Kr(4p^5 5p)$ + He or $Kr(4p^5 5p)$ + Ne mixtures for optically pumped lasers will be worthwhile.

AUTHOR INFORMATION

Corresponding Author

*Phone: 404 727 6617. Fax: 404 727 6586. E-mail: mheaven@emory.edu.

ACKNOWLEDGMENT

This work was supported by the Joint Technology Office through the Air Force Office of Scientific Research (AFOSR) under Contract FA9550-07-1-0572.

REFERENCES

(1) Beach, R. J.; Krupke, W. F.; Kanz, V. K.; Payne, S. A.; Dubinskii, M. A.; Merkle, L. D. *J. Opt. Soc. Am. B* **2004**, *21*, 2151.
(2) Zhdanov, B. V.; Shaffer, M. K.; Knize, R. J. *Proc. SPIE* **2010**, *7581*, 75810F/1.
(3) Readle, J. D.; Wagner, C. J.; Verdeyen, J. T.; Spinka, T. M.; Carroll, D. L.; Eden, J. G. *Proc. SPIE* **2010**, *7581*, 75810K/1.
(4) Komashko, A. M.; Zweiback, J. *Proc. SPIE* **2010**, *7581*, 75810H/1.
(5) Sulham, C. V.; Perram, G. P.; Wilkinson, M. P.; Hostutler, D. A. *Opt. Commun.* **2010**, *283*, 4328.
(6) Holmes, N. C.; Siegman, A. E. *J. Appl. Phys.* **1978**, *49*, 3155.
(7) Djeu, N.; Burnham, R. *Appl. Phys. Lett.* **1974**, *25*, 350.
(8) Hennecart, D. *J. Phys. (Paris)* **1978**, *39*, 1065.
(9) Hennecart, D.; Masnou-Seeuws, F. *J. Phys. B* **1985**, *18*, 657.
(10) Grandin, J. P.; Hennecart, D.; Husson, X.; Lecler, D.; Vienne, J. F.; Barrat-Rambosson, M. *J. Phys. (Paris)* **1975**, *36*, 787.
(11) Paterson, A. M.; Smith, D. J.; Borthwick, I. S.; Stewart, R. S. *J. Phys. B* **2001**, *34*, 1815.
(12) Chang, R. S. F.; Setser, D. W. *J. Chem. Phys.* **1980**, *72*, 4099.
(13) Arrathoon, R.; Sealer, D. A. *Phys. Rev. A* **1971**, *3* (4), 815.
(14) Bahrim, C.; Hennecart, D.; Kucal, H.; Masnou-Seeuws, F. *J. Phys. B* **1999**, *32*, 3091.
(15) Hennecart, D.; Barrat-Rambosson, M. *J. Phys. (Paris)* **1977**, *38*, 133.
(16) Manders, M. P. I.; Driessen, J. P. J.; Beijerinck, H. C. W.; Verhaar, B. J. *Phys. Rev. Lett.* **1986**, *57*, 1577.
(17) Manders, M. P. I.; Driessen, J. P. J.; Beijerinck, H. C. W.; Verhaar, B. J. *Phys. Rev. A* **1988**, *37*, 3237.
(18) Manders, M. P. I.; Ruyten, W. M.; Van den Beucken, F.; Driessen, J. P. J.; Veugelers, W. J. T.; Kramer, P. H.; Vredenbregt, E. J. D.; Van Hoek, W. B. M.; Sandker, G. J.; et al. *J. Chem. Phys.* **1988**, *89*, 4777.
(19) Batyrbekov, G. A.; Batyrbekov, E. G.; Danilychev, V. A.; Khasenov, M. U. *Kvantovaya Elektron. (Moscow)* **1990**, *17*, 1175.
(20) Chang, R. S. F.; Horiguchi, H.; Setser, D. W. *J. Chem. Phys.* **1980**, *73*, 778.
(21) Webster, M. J.; Shaw, M. J. *J. Phys. B* **1979**, *12*, 3521.
(22) Zayarnyi, D. A.; Kholin, I. V. *Quantum Electron.* **2003**, *33*, 474.